

Optical nutation in a collinear fast-ion-beam–laser experiment

A. Wännström, A. Kastberg, A. Arnesen, R. Hallin, C. Nordling, and O. Vogel
Department of Physics, University of Uppsala, Box 530, S-751 21 Uppsala, Sweden

S. Linnaeus

Department of Theoretical Physics, University of Uppsala, Thunbergsvägen 3, S-752 38 Uppsala, Sweden

(Received 23 May 1989)

Optical nutation in Ba II has been studied with a rapid Doppler-shifting technique in a cw collinear fast-ion-beam–laser experiment. Time-resolved nutation curves have been recorded as a function of transition, laser irradiance, laser frequency detuning, and laser polarization. Frequency spectra recorded at different, well-specified, times of interaction between the ions and the laser field reveal several interesting effects. Among them is the pronounced influence of the postacceleration potential on the line profiles. Theoretical curves, calculated in the density-matrix formalism, reproduce all the characteristics of the experimental data. Future possibilities of this technique are discussed, e.g., the prospects of determining transition probabilities through the measurements of optical nutation.

I. INTRODUCTION

When a strong laser field starts to interact resonantly, or near resonantly, with two-level atoms, the atoms will be coherently driven up and down between the two levels until different relaxation mechanisms, such as collisions and spontaneous emission, have damped out the population oscillations and steady state has been reached. Neglecting damping, the angular frequency Ω of this transient oscillation is given by

$$\Omega^2 = (\mathbf{D}_{1,2} \cdot \mathbf{E}_0 / \hbar)^2 + (\omega - \omega_0)^2,$$

where $\mathbf{D}_{1,2}$ is the matrix element of the electric dipole operator and \mathbf{E}_0 the amplitude of the laser electric field. The second term is the squared detuning between the laser field frequency ω , and the resonance frequency ω_0 . In the case of zero detuning Ω equals the Rabi frequency $\Omega_R = \mathbf{D}_{1,2} \cdot \mathbf{E}_0 / \hbar$, which was first introduced by Rabi.¹

This oscillation is often called optical nutation because it is the optical analogy of spin nutation. The analogy was not clear until Dicke² showed that transient electric-dipole transitions behave in the same way as spin transients of rf magnetic dipole transitions (e.g., the spin echo³ and the spin nutation⁴). This is the reason why the Bloch formalism⁵ is often used to describe these optical phenomena,⁶ although it was originally created to describe nuclear magnetic resonance.

Optical nutation was first seen by Hocker and Tang⁷ using an absorption band in gaseous SF₆ and pulses from a 10.6- μm Q-switched CO₂ laser. It was later demonstrated by Brewer and Shoemaker⁸ with a Stark-shift technique, and Farrell, MacGillivray, and Standage⁹ observed it using an electro-optical pulsed ring dye laser. Recently, Golub, Bai, and Mossberg¹⁰ have observed optical nutation, among other optical transient effects, in an atomic beam experiment. Many groups have seen Rabi oscillations by probing the population as a function of

laser field amplitude (or pulse length),^{11–15} rather than observing them in the time domain.

A number of different experimental techniques have been developed during the past two decades in order to study optical nutation and other (optical) coherent transients, such as photon echo and free induction decay. Recently, we reported the observation of optical nutation in a fast-ion-beam–laser experiment with a rapid Doppler-shift technique.¹⁶ In this paper, we bring the analysis forward, examine additional features of our experimental technique and demonstrate that the technique offers the possibility of direct determination of atomic transition probabilities.

II. EXPERIMENT

Figure 1 shows part of the experimental arrangement: An isotopically pure beam of ions is overlapped with the counterpropagating radiation from a single-mode cw ring dye laser (CR-699) with an effective bandwidth less than 1 MHz. The ions are rapidly Doppler shifted into resonance with the laser radiation when they experience the nonzero potential in a Faraday cage. In this work, transitions are induced between levels in the $5d$ and $6p$ configurations (see Fig. 2) in nuclear spin-free singly ionized ¹³⁸Ba. The degree of excitation of the upper level taking part in a transition is monitored by measuring the intensity of the spontaneously emitted, incoherent, light from this level down to the ground level. In this way one may observe time-resolved population variations simply by moving the light collector along the ion beam, as well as frequency-resolved spectra at any given time after the pulse onset by scanning the laser frequency with the light collector at a fixed position.

In order to observe nutation, some crucial prerequisites must be fulfilled.

(i) The time to shift the ions into resonance, i.e., the ion postacceleration time, must be short compared with the

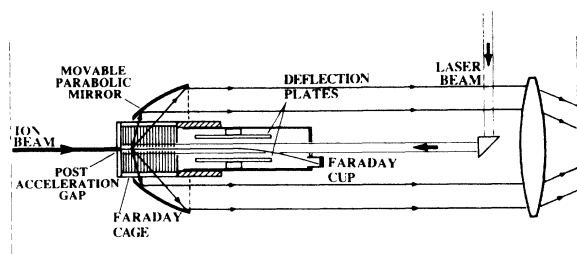


FIG. 1. Part of the experimental setup. Inside the Faraday cage the ions are Doppler tuned into resonance with the counterpropagating radiation. A time-resolved signal is obtained by moving the reflector along the ion beam, whereas a frequency-resolved signal is obtained by keeping the reflector at any given, fixed, position (i.e., time) and scanning the laser frequency.

lifetime.

(ii) The time resolution, i.e., the spatial resolution of the light-collecting system, must be sufficiently high so that the nutation pattern will not be smeared out. Also, the light-collecting system must have a high efficiency since low ion currents through small apertures have to be used (see below).

(iii) To prevent a broad distribution of nutation frequencies, the electric field amplitude of the laser light over the interacting volume of the ion beam must be approximately constant, and the longitudinal velocity distribution of the ions should be narrow.

(iv) The Rabi frequency, which increases with increasing laser field amplitude and transition probability, must

be of the order of or greater than the homogeneous linewidth of the transition.

The step rise time is determined by the velocity of the ions and the smoothly changing electrostatic potential between the entrance plate of the Faraday cage and the earthed plate in front of it. Due to the shape of this potential, the definition of a rise time becomes somewhat arbitrary, but a reasonable measure is the time between almost no interaction at all and almost resonant interaction. For instance, the time it takes for the center of the velocity distribution of ions to shift from 500 MHz off resonance to 30 MHz off resonance is less than 3 ns.

The time resolution is determined by the velocity of the ions as well as the optics of the photon counting system,¹⁷ which has been designed to give both high efficiency and high spatial resolution. The system consists of (see Fig. 1) a movable parabolic reflector, a converging lens, a broadband monochromator and a photomultiplier tube. The reflector collects fluorescence light from its focus with an acceptance angle of about 10% of the total solid angle and directs it to the photomultiplier tube through the lens and the monochromator. The spatial resolution along the ion beam of the movable detection system has been measured to be 0.30 ± 0.05 mm corresponding to a typical time window of about 1.3 ± 0.2 ns.

The ion beam is collimated (cf. Ref. 10) to a diameter of half a millimeter, and the freely expanding Gaussian laser beam produces at a distance of 3 m a spotsize inside the Faraday cage of about 2.4 mm. This reduces the variation of the laser field amplitude over the cross section of the ion beam, on which the laser beam is centered, to less than 1%.

The kinematic compression of the longitudinal velocity distribution in a fast ion beam^{18,19} is essential for the experiment. The Doppler contribution to the observed linewidth at low laser power (less than 1 mW) has been determined by fitting a frequency scan over the transition to a Voigt profile, where the Lorentzian contribution is known very accurately due to the accurate lifetimes available for these levels. The result is a Doppler width of 35 MHz, which is sufficiently narrow in order to efficiently use all atoms in the beam; i.e., most atoms will contribute to the signal recorded. The additional damping due to this inhomogeneous line-broadening mechanism is small.

Finally, the laser power densities required for nutation periods in the nanosecond range are easily obtained with the ring dye laser for the transitions studied here, producing Rabi frequencies of the order of 50–100 MHz to be compared with the homogeneous linewidths of 20–25 MHz. It should be noted that in a fast-ion-beam experiment, the only important homogeneous damping mechanism is the spontaneous emission. This is due to the low density of the ion beam and the low rest gas pressure in the experimental chamber.

Having fulfilled all the essential conditions, nutation curves are recorded by the following procedure: The light collector is placed far downstream from the entrance of the Faraday cage where the electrostatic potential is close to its asymptotic value. Then the laser frequency is set to the center of the resonance peak of the actual transition with the laser irradiance strongly re-

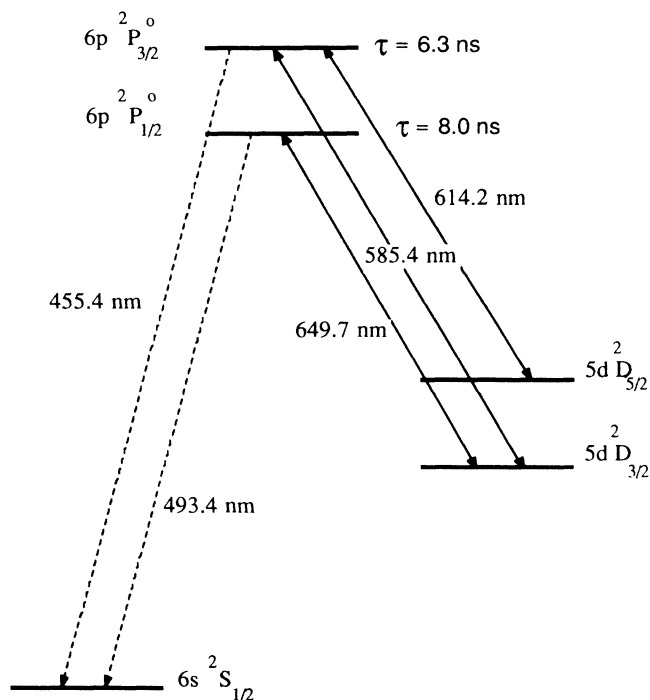


FIG. 2. Level scheme of Ba II indicating lifetimes and the transitions used. The transition probabilities are from Ref. 23 (in units of 10^8 s^{-1}); transition 1 (585.4 nm), 0.048; transition 2 (614.2 nm), 0.37; transition 3 (649.7 nm), 0.332.

duced with filter to avoid power broadening and suboptimizing on any sidewing that appears at high intensities. This procedure defines zero detuning. Measurements at arbitrary detunings (any multiple of 10 MHz) is obtained by changing the offset of the ring dye-laser scan control. The irradiance is measured, between runs, with a calibrated diode inserted behind the entrance aperture of the Faraday cage. A nutation curve is recorded in two minutes after positioning the reflector to an appropriate starting point. Since the reflector moves continuously during a recording, the time resolution decreases from 1.3 to 1.7 ns.

Frequency-resolved spectra are recorded by positioning the movable reflector at any given fixed position (i.e., time) after the postacceleration region and scanning the frequency of the laser. A more detailed discussion of the experimental parameters is undertaken in Sec. V.

III. THEORY

Our description of the observed nutation is based on the density-matrix formalism.²⁰ The result for an idealized two-level atom where spontaneous emission has been neglected has already been given. In our experiment, however, both of the two levels are degenerate, corresponding to different orientations of the dipole moment, where the different states are denoted by the magnetic

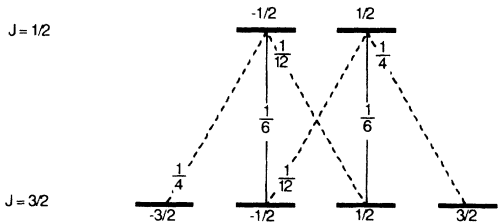
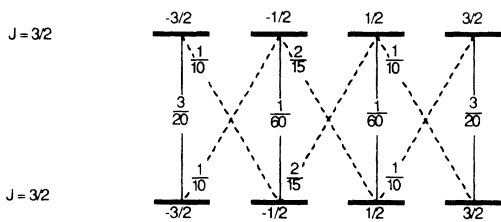
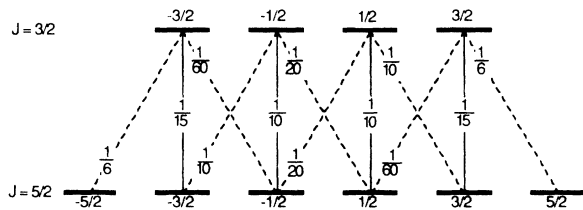


FIG. 3. Diagrams showing the relative intensities for transitions between different states. It is clear that the only transition with one Rabi frequency in this part of the Ba II level scheme is the $J = \frac{3}{2} \rightarrow J = \frac{1}{2}$ transition using linearly polarized light and hence only $\Delta m = 0$ transitions.

quantum number m . Furthermore, the spontaneous emission is substantial (see Fig. 2). These effects have to be included in any attempt to reproduce experimental data.

The laser induces transitions between two degenerate levels, which we denote 1 and 2, 1 being the lower level which is metastable. Since the laser light is linearly polarized, only $\Delta m = 0$ transitions are induced. The population numbers of the $2m$ states $\rho_{2m,2m}$ will oscillate with different Rabi frequencies since the dipole moment $\mathbf{D}_{1m,2m}$ depends on the magnetic quantum number m (see Fig. 3 and Ref. 21).

A proper treatment of the spontaneous emission must be based on quantization of the radiation field, which is described, e.g., by Stenholm.²² We give in the appendix a treatment where the degeneracy of the levels is explicitly taken into account. As concerns the diagonal density-matrix elements (i.e., the population numbers), one finds that the spontaneous decay rates enter in the equations exactly as could be expected from a phenomenological point of view, causing damping of the oscillations as well as coupling between different m values via $\Delta m = \pm 1$ transitions. A less predictable result is that the nondiagonal matrix elements decay spontaneously with half the decay rate of the upper level (when the lower level is metastable). Thus the equations of motion for the density-matrix elements take the form

$$\frac{d\rho_{1m,1m}}{dt} = -v_m \tilde{\rho}_{1m,2m} - v_m^* \tilde{\rho}_{2m,1m} + 2 \sum_{m'} \gamma_{m',m} \rho_{2m',2m'},$$

$$\frac{d\rho_{2m,2m}}{dt} = v_m \tilde{\rho}_{1m,2m} + v_m^* \tilde{\rho}_{2m,1m} - 2\gamma \rho_{2m,2m},$$

$$\frac{d\tilde{\rho}_{1m,2m}}{dt} = v_m^* (\rho_{1m,1m} - \rho_{2m,2m}) + (i\Delta - \gamma) \tilde{\rho}_{1m,2m},$$

where Δ is the detuning, γ the total decay rate from either of the states $2m$, $\gamma_{m',m}$ the decay rate of the particular transition $2m' - 1m$, and

$$v_m = \frac{i}{2\hbar} \mathbf{E}_0 \cdot \mathbf{D}_{1m,2m},$$

$$\tilde{\rho}_{1m,2m} = e^{-i\omega t} \rho_{1m,2m},$$

$$\tilde{\rho}_{2m,1m} = \tilde{\rho}_{1m,2m}^*.$$

The decay rate γ is given by the lifetime τ of the upper level through

$$\gamma = 1/2\tau.$$

For the specific decay rate $\gamma_{m',m}$ we obtain from the Wigner-Eckart theorem

$$\gamma_{m',m} = \frac{(2j_2 + 1)\beta}{2\tau} \begin{pmatrix} j_1 & 1 & j_2 \\ -m & m - m' & m' \end{pmatrix}^2,$$

where β is the branching ratio for transitions from level 2 to level 1 and j_1 and j_2 are the angular momenta of the two levels. Using the well-known expression for the transition probability in terms of the dipole moment, one can derive the following expression for the absolute value of v_m :

$$|v_m|^2 = \frac{3\pi c^2 I}{\hbar \omega_{21}^3} \gamma_{m,m},$$

where I is the irradiance of the laser beam. Since the phase of v_m only influences the phase of the nondiagonal density-matrix elements, one can, without altering the physically measurable quantities, take v_m real and positive. Hence all atomic parameters needed to calculate the density matrix are the transition wavelength, the lifetime of level 2 and the branching ratio for the transition to level 1.

From the equations above we find that an analytical solution for the density-matrix elements can be found in the form

$$\rho_{1m,1m} = \sum_i a_{m,i} e^{\lambda_i t},$$

$$\rho_{2m,2m} = \sum_i b_{m,i} e^{\lambda_i t},$$

$$\tilde{\rho}_{1m,2m} = \sum_i c_{m,i} e^{\lambda_i t},$$

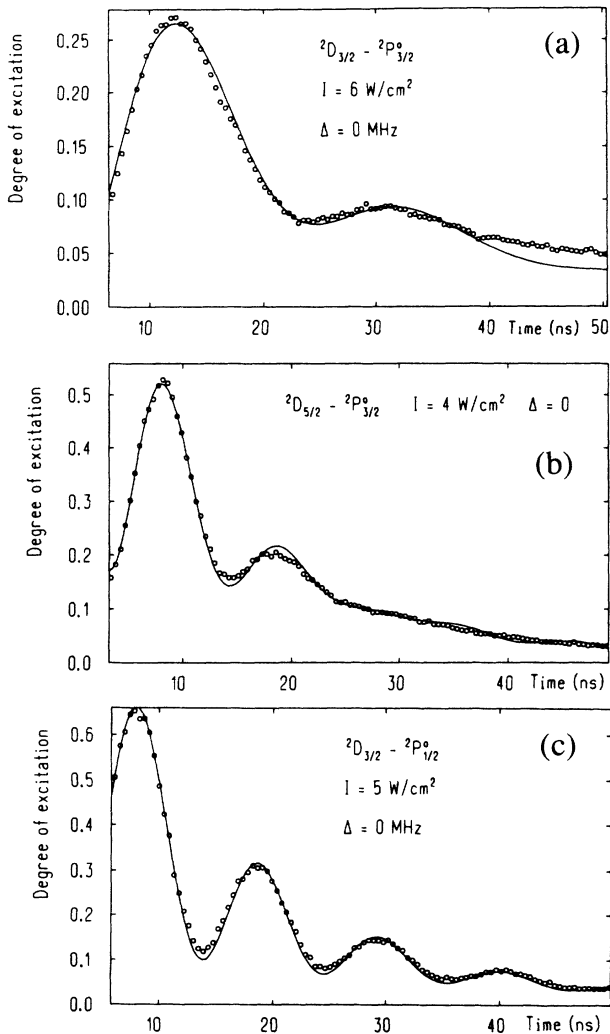


FIG. 4. Dependence of nutation on dipole moment $D_{1,2}$ using linearly polarized light ($\Delta m = 0$ transitions). The solid line is the calculated curve.

where λ_i and the coefficients $a_{m,i}$, etc., are complex numbers to be determined from a matrix eigenvalue equation.

During the postacceleration the ions experience a time-dependent detuning. By writing the Schrödinger equation in a coordinate system moving with the ions, one finds that the equations of motion for the density matrix in the form written above remain valid provided one makes the definition

$$\tilde{\rho}_{12} = \exp \left[i \int \mathbf{k} \cdot \mathbf{v}(t) dt - i \omega t \right] \rho_{12}$$

and replaces Δ by the Doppler shifted detuning Δ_D given by

$$\Delta_D(t) = \Delta - \omega v_k(t)/c.$$

In general, one cannot solve the density-matrix equations analytically in the postacceleration region. The equations are therefore solved numerically in this region, but when the asymptotic value of the potential is approached, an analytical solution is applied.

IV. RESULTS

A. Time-resolved spectra

Experimental curves have been produced with the transitions indicated in Fig. 2 using different laser field amplitudes, different detunings as seen by the ions in the beam, and different polarizations of the laser light. Figures 4–7 show observed optical nutation under varying

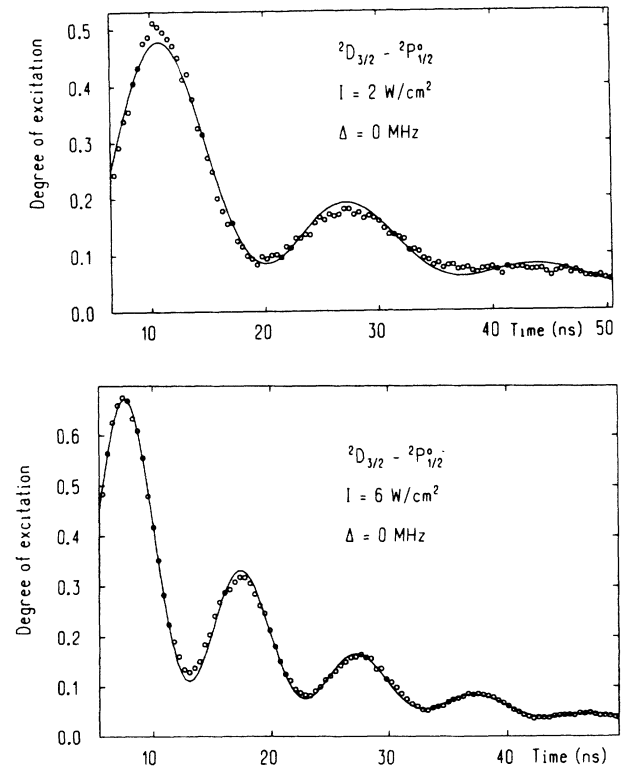


FIG. 5. Dependence of nutation on laser field strength E_0 using transition 3 and linearly polarized light ($\Delta m = 0$ transitions). The solid line is the calculated curve.

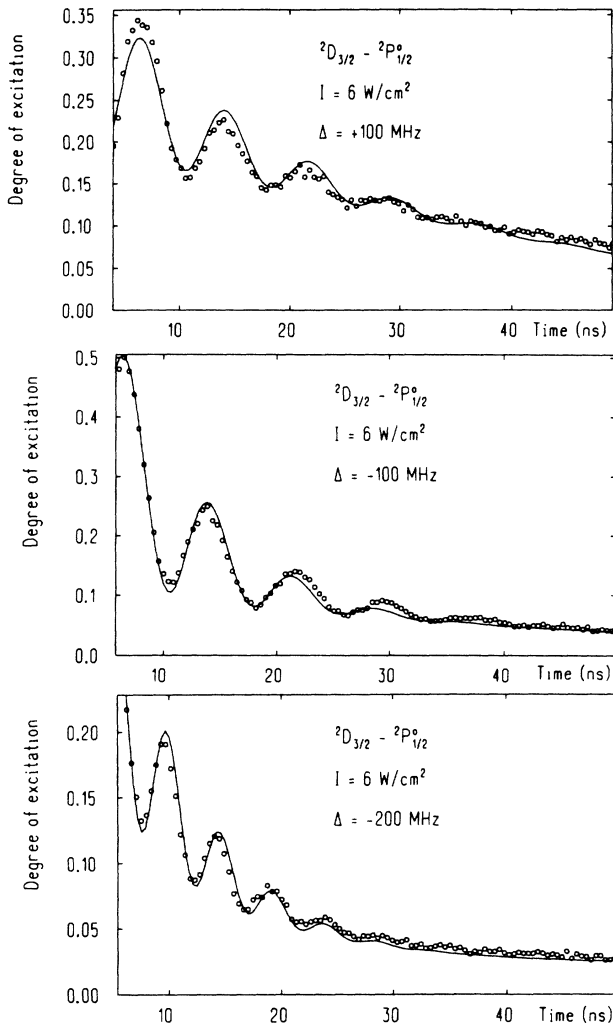


FIG. 6. Dependence of nutation on laser frequency detuning (Δ) using transition 3 and linearly polarized light ($\Delta m = 0$ transitions). The solid line is the calculated curve.

experimental conditions. Each curve is the added experimental data of three to seven individual runs. The observations agree qualitatively with the simple two-level model. Figure 4 illustrates the influence of the degeneracy, showing the difference between cases with only one Rabi frequency present (c) and two Rabi frequencies (a)- and (b), which interfere and smear out the oscillations (cf. Fig. 3). Figures 5 and 6 show the increase of nutation frequency with increasing laser field amplitude and detuning. Figure 7 reveals a dramatic difference of the effect on nutation curves between circularly and linearly polarized light. The difference is easily explained from Fig. 3 where it is seen that for $\Delta m = 0$, two different Rabi frequencies are present whereas in the $\Delta m = +1$ case there are four different Rabi frequencies interfering, thus inhibiting the observation of distinct nutation.

In order to perform a quantitative comparison with theory, nutation curves were calculated (Figs. 4–7 as solid curves). The effect of the velocity distribution of the ions and the shape of the time window have been taken

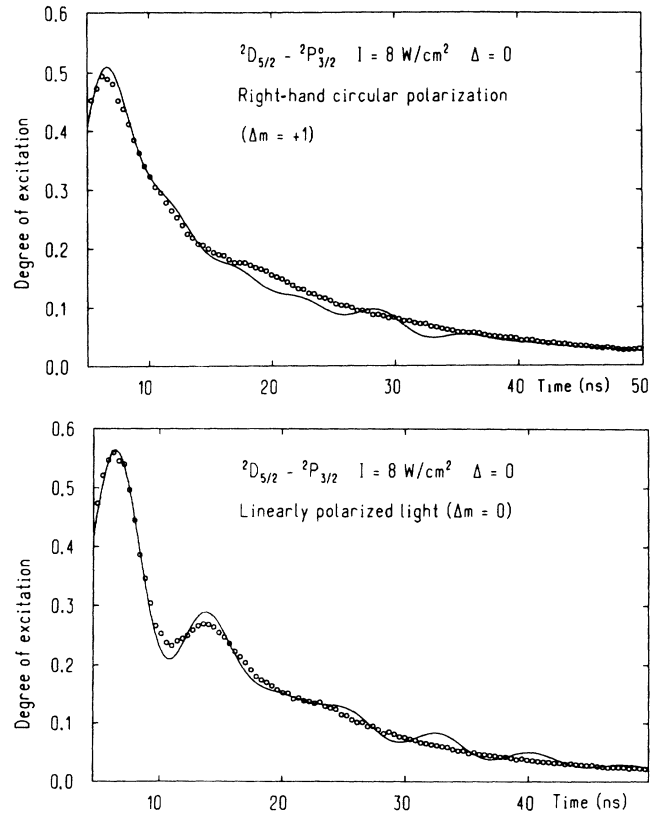


FIG. 7. Dependence of nutation on laser polarization using transition 2. The solid line is the calculated curve.

into account as well as the postacceleration potential function. The value of the dipole moments have been taken from the literature²³ and have been kept fixed in the calculations, whereas the laser power density and the detuning have been allowed to vary to obtain a good least-squares fit. This procedure is motivated by the relatively large uncertainties in laser power density ($\approx 20\%$) and detuning (≈ 20 MHz) in the present measurements compared with the uncertainty of the dipole moments ($\approx 10\%$). Within these error limits the theory describes the observations well. The only other free parameters used in the least-squares fit were a normalization parameter and the zero point for the time scale. The necessity to include the postdeceleration potential is dramatically visualized in Fig. 6. The asymmetry between negative and positive detuning can only be explained by the influence of the potential. We have used a positive potential and therefore, with negative detuning, the ions will be postdecelerated across the resonance before measurements start, whereas this will not happen with a positive detuning. This creates different initial conditions for the two cases and hence an asymmetry.

B. Frequency-resolved spectra

The frequency-resolved spectra exhibit transit time broadening and optical pumping as well as other interesting characteristics. These spectra can also be used to obtain information on the effect of the postacceleration potential on the observed features in the time-resolved

recordings. The theoretical curves presented are calculated from nominal data of all parameters, i.e., no least-squares fit have been applied. Two separate cases will be discussed: the regime of low laser power and the one of high laser power.

Low laser power. The laser power in these recordings has been below 1 mW, which corresponds to an irradiance below 0.05 W/cm^2 . As can be seen in Fig. 8 the width of the transition increases with decreasing interaction time, which is an effect of transit time broadening. Moreover, Fig. 9(a) shows that not only does the width change with the distance, but also the peak position changes with approximately 90 MHz over a distance corresponding to some 10 ns. This phenomenon is further illustrated in Fig. 9(b) where the time development of the degree of excitation is calculated at low intensities. Close to the postacceleration potential gap negative detuning yields a higher degree of excitation than zero detuning, which moves the peak towards negative detuning. Note that these curves all display a change in the peak position even when the asymptotic value of the postacceleration potential has already been reached within 1 V, corresponding to a detuning of a few megahertz. Hence the slightly varying detuning in this region, due to the slowly changing potential, is not responsible for the peak shift;

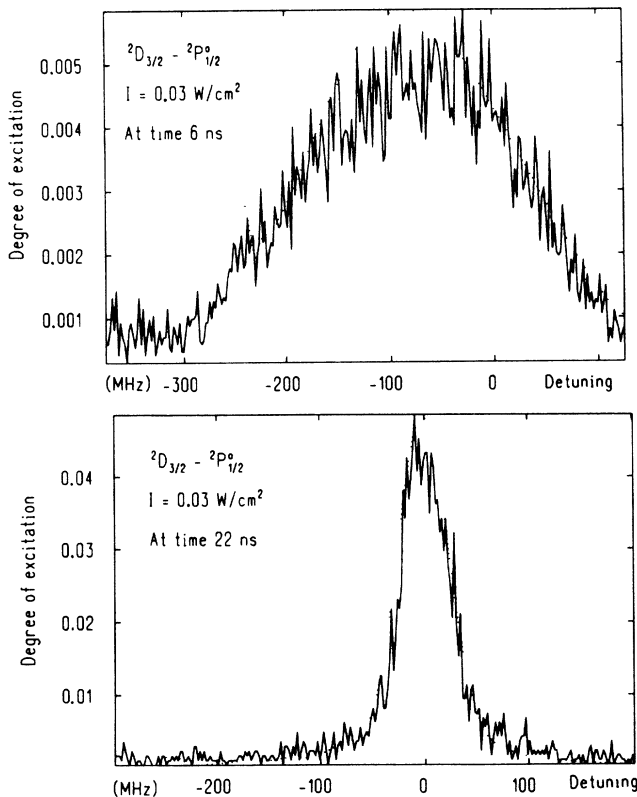


FIG. 8. Frequency spectra of transition 3 at two different interaction times using very low irradiance and linearly polarized light. Dotted curves are theoretical spectra calculated from nominal values on all parameters.

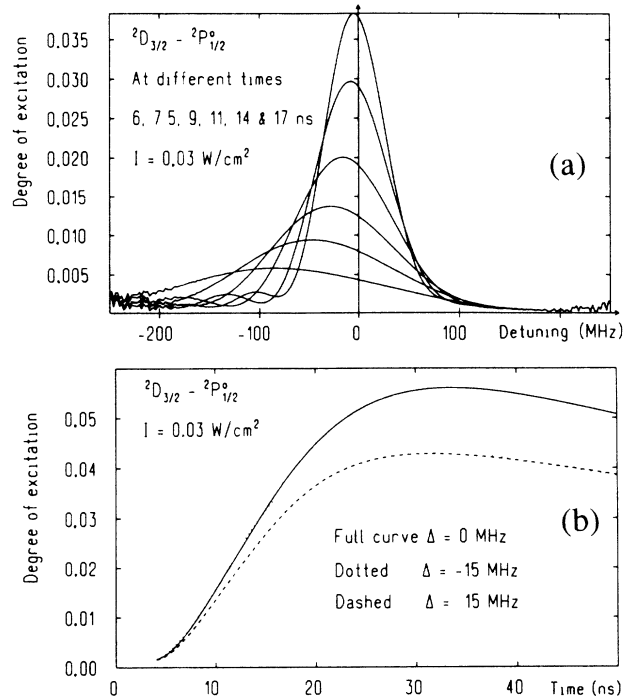


FIG. 9. (a) Theoretical frequency spectra of transition 3 at very low laser irradiance and (b) the corresponding time developments at different, fixed, detunings.

rather, this is a consequence of the nonadiabatic Doppler switching that occurs (cf. the discussion in Sec. VI). The spectrum would be shifted to the positive side if the potential had been negative instead of positive. One may conclude that in order to obtain a correct and well-defined detuning avoiding line shifts and broadenings when setting the resonance frequency, one should be far away from the postacceleration gap. It is worth noting that this also holds for isotope shift and hyperfine structure measurements using collinear fast-ion-beam-laser spectroscopy.

High laser power. The sequence of frequency scans in Figs. 10 and 11 shows some distinct features. The asymmetry, i.e., the long wing on the low-frequency side, is obvious—as well as the dip appearing after a long interaction time. This asymmetry can again be understood from the postdeceleration. With negative detuning, ions will be in resonance with the laser field somewhere in the gap, before entering the detection region, whereas this will not happen with positive detuning. The dip is due to optical pumping, i.e., ions at resonance are more efficiently transferred, via spontaneous emission from the excited level, to the ground state where they are lost from further interactions with the laser field (cf., e.g., Refs. 24 and 25). There is a good agreement between the experimental and the theoretical curves, which indicates that the postacceleration potential, as well as the velocity distribution, has been taken into account in a satisfactory way.

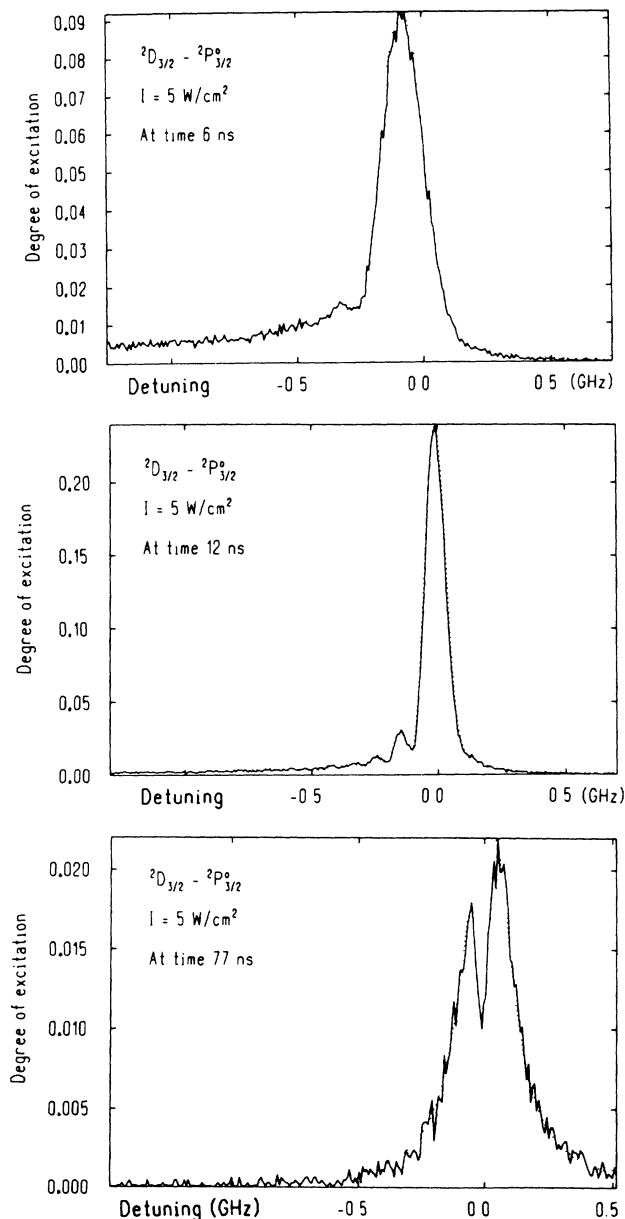


FIG. 10. Frequency scans of transition 1 after different interaction times using 5 W/cm² and linearly polarized light. Dotted curves are theoretical spectra calculated from nominal values on all parameters. Observe the structure at the low-frequency side and the optical pumping encountered after long interaction times with the laser.

V. MEASUREMENTS OF TRANSITION PROBABILITIES

A. Introduction

In this section we suggest a method based on optical nutation for deriving atomic transition probabilities. The optical Rabi frequency $\Omega_R = \mathbf{D}_{1,2} \cdot \mathbf{E}_0 / \hbar$ is a measure of the interaction strength between an atom and an optical field. A measurement of the Rabi frequency will there-

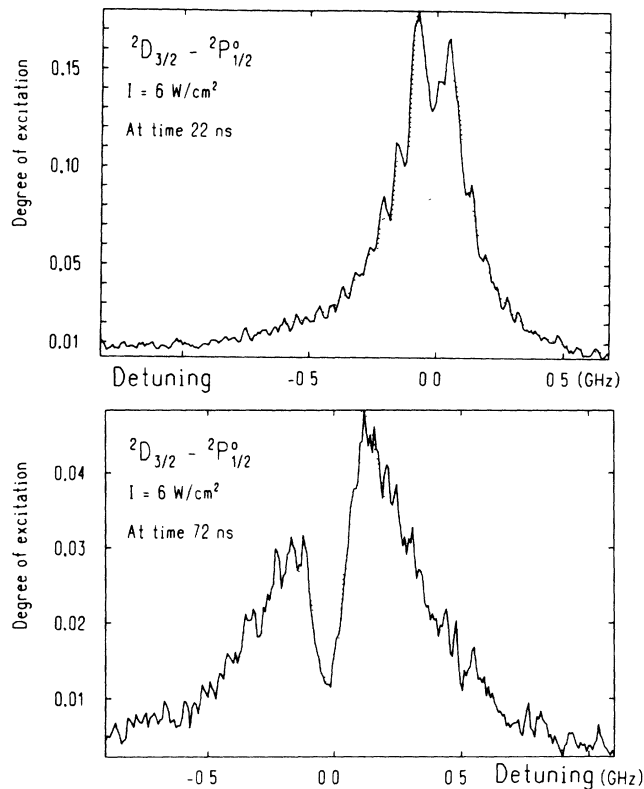


FIG. 11. Frequency scans of transition 3 after different interaction times using 6 W/cm² and linearly polarized light. Dotted curves are theoretical spectra calculated from nominal values on all parameters.

fore, regardless of its manifestation, give the dipole moment and hence the transition probability directly, provided that the optical field amplitude can be determined. This idea has already been used by several groups working in a steady-state environment^{26–28} in order to determine transition probabilities. Scarl *et al.*¹² measured a dipole-matrix element for a transition in ²³⁸U observing damped Rabi flopping as a function of the laser irradiance of a resonant pulse of fixed duration. Adam *et al.*¹⁵ determined dipole moments in CH₃F with the same principle reaching an accuracy of 5%. Direct measurements of transition dipole-matrix elements using time-resolved optical nutation have been made by Shoemaker and van Stryland²⁹ on molecular transitions in the microsecond time range using the Stark switching technique, where accuracies of 5–8% were obtained. It is clear that also the method of observing optical nutation described in this work should allow the determination of transition probabilities with good accuracy. To assess the advantages of the technique, a discussion follows of all the features in our experiment that may affect such determinations.

B. Experimental considerations

The frequency of the nutation pattern does not directly correspond to the Rabi frequency since damping and other mechanisms (e.g., the degeneracy) change the pattern.

Therefore, in order to determine transition probabilities from nutation data, a least-squares fit has to be made with only one free parameter apart from the normalization parameters mentioned previously, namely, the transition probability. However, if the branching out of the system is not negligible, which is true for all practical cases with our technique, the residual branching enters as a free parameter as well, unless the lifetime of the upper level is known. If the lifetime is not known, it can be measured with the time-of-flight method.³⁰ The idea here is that with this method it is possible to determine the transition probability for a given transition without having complete knowledge of all the branching ratios. The uncertainties in the time scale and the irradiance have a simple relation to the uncertainty in the transition probability, but the other experimental parameters that determine the shape of a nutation curve do not, i.e., the time resolution, the spatial intensity distribution of the laser light, the Doppler width, the detuning, and the post-acceleration potential. To explore their relations, these parameters, except for the spatial intensity distribution, have been varied systematically in least-squares fits of theoretical nutation curves to experimental ones. It turns out that these latter parameters contribute only marginally, or may be controlled to give only small contributions, to the uncertainty in the transition probability. In general, the importance of these parameters is reduced with increasing Rabi frequency. Below a discussion follows of the different parameters that may influence the uncertainty in transition probabilities derived from nutation curves.

C. Time scale and time resolution

The total uncertainty in the time scale is 0.54% (Ref. 30) and may produce a small systematic error in the determination of a transition probability. It will be of negligible importance compared with other sources of error.

The uncertainty of 12% in the value of the finite time resolution will not affect a transition probability derived from data more than 2.7%. This uncertainty is, of course, easily reduced if so is necessary.

There is a small variation of detection efficiency along the ion beam³⁰ which, also when taken into account, gives a residual uncertainty to the determinations of transition probabilities. This uncertainty is well below 0.2%

D. Laser irradiance and laser beam profile

The irradiance of the laser light is the most important experimental parameter. Presently, the uncertainty in the irradiance is too high (20%) to admit an improvement of the accuracy of any of the dipole moments in the transitions used here. However, power meters with absolute accuracies as high as 1% are commercially available, contributing only 0.5% to the uncertainty in the transition probability.

The inherent power noise from the dye laser is, according to specifications, 2.5% (root-mean-square value in the region 10 Hz–100 kHz) and since the dye laser will reflect power fluctuations from the pump laser, specified

to be less than 1%, a power ripple of 3–4% can be expected, adding a Gaussian damping to the nutation curves. Since the power ripple has not been measured, it is not included in the calculations and will, therefore, introduce a small error to the transition probabilities determined. This ripple can be reduced by active stabilization.

The intensity profile is expected to be flat over the interaction region within approximately 1%. With our present power measurements, it is not possible to determine the profile with any corresponding accuracy and it may therefore be less flat than estimated. Laser-field inhomogeneities may therefore be an additional, but small, damping source.

E. Doppler width and detunings

The dominant contribution to the Doppler width is probably the acceleration voltage ripple of around 6 V. This could, of course, be improved with a more stable power supply. The uncertainty of 11% in the Doppler width only introduces a 0.7% uncertainty in the determination of a transition probability. Beam misalignments could also contribute to the overall Doppler width, but in this setup a beam overlap within a few mrad is easily obtained and hence this contribution is less than a few megahertz.

In these measurements, the Rabi frequency has been of the order of 50–100 MHz and the detuning is therefore important. Here Fig. 9(a) might be recalled, which showed that the detuning has to be set with some care, i.e., optimization should be carried out far away from the excitation region. In such cases, the transition is centered within 5 MHz.

However, the detuning may change during an experiment. This is the reason for recording our data in a short time to limit the effects of a gradually changing acceleration voltage, which is the main cause of detuning variations.

A small drift in the accelerating voltage of 0.015% (5 V) changes the detuning with 25 MHz and therefore also the nutation pattern. Monitoring the ion current through the 0.49-mm aperture during an experiment provides a method of checking voltage drifts provided the deflective magnetic field is stable. The sensitivity of this method depends on the dispersion of the electromagnetic separator. Perpendicular to the beam at focus, the dispersion is 19 mm/amu at 100 amu, corresponding to an estimated 18 V/mm, or 90 MHz/mm, at 32 kV. With an ion beam full width at half maximum diameter of 5 mm, this means that the detuning has been stable within 20 MHz if the current has not changed with more than $\pm 3\%$. In general, the current has been extremely stable.

The best solution is to stabilize the detuning. Various schemes can be found in the literature, e.g., that of Hühnermann *et al.*,³¹ who lock the frequency of the laser to any other isotope present in an auxiliary beam line. Their scheme demands a good short-time stability; i.e., ripple and noise of the acceleration voltage should be below 0.5 V. If that condition can be fulfilled, their scheme can stabilize to below 1 MHz.

An error in the detuning of 10–20 MHz would change

the derived value of a transition probability with 5–20 % depending on the sign of the detuning as well as transition and Rabi frequency. If one allows the detuning to vary as a free parameter, the fitted value of the detuning never changes more than approximately 10 MHz, whatever other parameters are varied. With a stabilization scheme, this error would become almost insignificant.

The shape of the post acceleration potential is not known exactly, but the good agreement between the theoretical and the experimental spectra indicates that it is taken into account in a satisfactory way. The voltage itself is known very accurately. Simulating a change in the shape of the potential by varying the voltage with as much as 10% does not change the value of the transition probability with more than 1.8%.

F. Other parameters

Besides the primary parameters mentioned, static electric and magnetic fields may affect the optical nutation curves. A fairly strong, smoothly varying electric field is present in the postacceleration region. Consequently, the Stark effect has to be considered since significant shifts and splittings would mean an additional detuning mechanism in the postacceleration gap. The Stark effect of the levels in our experiment were estimated using tabulated transition probabilities for all significant contributors.²³ The maximum polarizability found was only 7 kHz/(kV/cm)² and since the electric field has a maximum value of 7.5 kV/cm, the Stark effect is in the order of 100 kHz and therefore totally negligible.

There is a weak stray magnetic field measured to be less than 0.1 mT. This will, in principle, remove the degeneracy, and may even produce additional beats. The g_j values are typically 1 for the studied levels and the corresponding Zeeman splitting is roughly 1.5 MHz. This splitting is not observable, but produces beats in the order of 300–400 ns, which would perturb our measurements if the amplitude of the beats were significant. There is no sign of deviations in our curves which could correspond to beats, and that indicates that the experimental geometry is advantageous for this kind of measurements. The removed degeneracy will not affect the calculations since the splitting is small compared to the homogeneous width of the transitions used.

The preceding discussion has shown that the only two experimental parameters, which presently introduce substantial errors in a transition probability determination, are the irradiance and the detuning. With the Rabi frequencies obtained in our experiments, the best solution at the present time will be to allow the detuning to vary as a free parameter within error bars simultaneously with the transition probability in a fit to experimental data. This is motivated by the fact that these two parameters affect the shape of the nutation curves in slightly different ways. This will result in a final uncertainty of 23% with quadratic addition. Reducing the uncertainty in irradiance by a factor of 10 with a precision power meter and stabilizing the detuning within 1 MHz will result in a total uncertainty of the transition probability below 8% with linear error addition, whereas a quadratic addition yields an uncertainty below 4%.

VI. DISCUSSION

We have demonstrated the possibilities which the rapid Doppler-shift technique in collinear fast-ion-beam–laser spectroscopy offers in studying optical transient effects, in particular, the possibilities to study “simultaneous” time- and frequency-resolved phenomena. The asymmetric consequences of a postacceleration potential have been investigated.

Future developments are possible. For instance, it is possible to introduce a second laser that couples the upper level to a higher-lying level. Provided that this extra coupling is weak compared with the coupling of the initial two-level system, probe spectra could be obtained by observing the fluorescence decay from the introduced probe level. Such probe spectra would show a splitting of the upper level into a doublet. This doublet is the well-known Autler-Townes doublet,³² first observed in the optical region by Refs. 33 and 34. The effect is generally known as the ac Stark effect. A lot of work, experimental as well as theoretical, has been devoted to the study of Autler-Townes spectra during the past decade,³⁵ but until recently³⁶ no one had investigated what happens directly after the instant the splitting field is turned on until the time where the doublet, which is a steady-state structure, has been fully developed. One reason for this is that Heisenberg’s uncertainty relation imposes limits on the resolution when one makes simultaneous measurements of time and frequency. Bai, Mossberg, and Berman³⁶ solved this problem in an elegant fashion simply by studying the time development of one probe frequency at a time with a detector coupled to a transient digitizer. It is quite clear from our earlier discussion that with our time resolution, which is one order of magnitude higher than that of Bai, Mossberg, and Berman, we could proceed further and study the transient development of the ac Stark effect by studying the probe-frequency spectra with the detector placed at one position at a time. The velocity of the ions gives the time scale and time-resolved ac Stark spectra are obtained. In such experiments the initial conditions could be varied simply by letting the ions experience short excitation pulses prior to the turn on of the driving field, i.e., by introducing further potential steps. It is clear that this would simultaneously reveal the response of optical nutation to different initial values.

Another interesting feature that could be investigated is the amount of adiabatic following^{37,38} introduced by the finite turn-on time of the exciting field. This is when the detuning changes slowly enough for the atomic system to adjust its level population smoothly while it is tuned into resonance. In Bloch’s vector formalism (see, e.g., Ref. 37) this corresponds to the case when the pseudomoments of the ions remain aligned along the effective field of the laser light in the rotating frame. With Rabi frequencies and relaxation times of the order of magnitude as in the present paper these effects can not be seen, but they should be visible with higher power densities or with atomic transitions with large dipole moments. Adiabatic following may be of importance for all fields of collinear laser ion-beam spectroscopy where slow postac-

celerations are being used. These effects could, with a few modifications, be studied with our setup. Finally, with commercially available power meters with absolute accuracies in the order of 1% this method, based on measurements of optical nutation, may be possible to use to measure transition probabilities with an accuracy of a few percent.

ACKNOWLEDGEMENTS

We would like to thank F. Heijkenskjöld for his assistance during the experiments. This work has been supported by the Swedish Natural Science Research Council (NFR).

APPENDIX: QUANTUM-MECHANICAL DERIVATION OF THE EQUATIONS OF MOTION FOR THE DENSITY MATRIX

The problem of Rabi oscillations in a quantized field can be treated in several different ways. We shall here apply the Schrödinger picture to retain some resemblance of the nonquantized field treatment, although the Heisenberg picture is more formally elegant. Thus the time evolution of the atom-radiation system is governed by the Schrödinger equation with a Hamiltonian of the form

$$\hat{H} = \hat{H}_{\text{atom}} + \hat{H}_{\text{int}} + \hat{H}_{\text{rad}} . \quad (\text{A1})$$

Applying the dipole approximation of the interaction energy we obtain for the three parts of the Hamiltonian

$$\hat{H}_{\text{atom}} = \hbar \sum_{\mu} \omega_{\mu} |\mu\rangle \langle \mu| , \quad (\text{A2a})$$

$$\hat{H}_{\text{int}} = i\hbar \sum_{\mathbf{k}} \sum_{\mu, \nu} (\hat{a}_{\mathbf{k}} - \hat{a}_{\mathbf{k}}^{\dagger}) g_{\mathbf{k}\mu\nu} |\mu\rangle \langle \nu| , \quad (\text{A2b})$$

$$\hat{H}_{\text{rad}} = \hbar \sum_{\mathbf{k}} \omega_{\mathbf{k}} \hat{n}_{\mathbf{k}} \equiv \hbar \hat{\Omega} , \quad (\text{A2c})$$

where we have used the notation

$$g_{\mathbf{k}\mu\nu} = \mathbf{f}_{\mathbf{k}} \cdot \mathbf{D}_{\mu\nu} , \quad (\text{A3})$$

with

$$\mathbf{f}_{\mathbf{k}} = \left[\frac{\omega_{\mathbf{k}}}{2\epsilon_0 \hbar V} \right]^{1/2} \boldsymbol{\epsilon}_{\mathbf{k}} . \quad (\text{A4})$$

We write the total wave function for the atom-radiation system

$$\psi(\mathbf{r}, t) = \sum_{\mu} |\xi_{\mu}(t)\rangle |\mu(\mathbf{r})\rangle , \quad (\text{A5})$$

where the ‘‘coefficients’’ $|\xi_{\mu}\rangle$ are wave functions in radiation space which can in their turn be expanded in terms of the number eigenstates:

$$|\xi_{\mu}\rangle = \sum_{\{n_{\mathbf{k}}\}} c_{\mu\{n_{\mathbf{k}}\}}(t) |\{n_{\mathbf{k}}\}\rangle . \quad (\text{A6})$$

Inserting the expansion (A5) into the Schrödinger equation, we obtain the following set of coupled equations for $|\xi_{\mu}\rangle$:

$$\begin{aligned} \frac{d|\xi_{\mu}\rangle}{dt} = & -i(\hat{\Omega} + \omega_{\mu})|\xi_{\mu}\rangle \\ & + \sum_{\mathbf{k}} \left[(\hat{a}_{\mathbf{k}} - \hat{a}_{\mathbf{k}}^{\dagger}) \sum_{\nu} g_{\mathbf{k}\mu\nu} |\xi_{\nu}\rangle \right] , \end{aligned} \quad (\text{A7})$$

which can also be written in the integral form

$$|\xi_{\mu}(t)\rangle = e^{-i(\hat{\Omega} + \omega_{\mu})t} \left[|\xi_{\mu}(0)\rangle + \int_0^t e^{i(\hat{\Omega} + \omega_{\mu})\tau} \sum_{\mathbf{k}} \left[(\hat{a}_{\mathbf{k}} - \hat{a}_{\mathbf{k}}^{\dagger}) \sum_{\nu} g_{\mathbf{k}\mu\nu} |\xi_{\nu}(\tau)\rangle \right] d\tau \right] . \quad (\text{A8})$$

Setting the coupling constants $g_{\mathbf{k}\mu\nu}$ equal to zero, we obtain the *zeroth-order* solution

$$|\xi_{\mu}(t)\rangle = e^{-i(\hat{\Omega} + \omega_{\mu})t} |\xi_{\mu}(0)\rangle . \quad (\text{A9})$$

Feeding this solution into the integral in (A8) we obtain the *first-order* solution

$$|\xi_{\mu}(t)\rangle = e^{-i(\hat{\Omega} + \omega_{\mu})t} \left[|\xi_{\mu}(0)\rangle + \int_0^t e^{i(\hat{\Omega} + \omega_{\mu})\tau} \sum_{\mathbf{k}} \left[(\hat{a}_{\mathbf{k}} - \hat{a}_{\mathbf{k}}^{\dagger}) \sum_{\nu} g_{\mathbf{k}\mu\nu} e^{-i(\hat{\Omega} + \omega_{\nu})\tau} |\xi_{\nu}(0)\rangle \right] d\tau \right] . \quad (\text{A10})$$

The time-dependent operators can be moved outside the integral sign by means of the commutation relation

$$\hat{a}_{\mathbf{k}} e^{\hat{n}z} = e^{(\hat{n} + \omega_{\mathbf{k}})z} \hat{a}_{\mathbf{k}} , \quad (\text{A11})$$

which is valid for any complex number z . Thus, evaluating the integral, we get

$$|\xi_{\mu}(t)\rangle = e^{-i(\hat{\Omega} + \omega_{\mu})t} \left[|\xi_{\mu}(0)\rangle + \sum_{\mathbf{k}} \sum_{\nu} i g_{\mathbf{k}\mu\nu} \left[-\frac{e^{i(\omega_{\mu\nu} - \omega_{\mathbf{k}})t} - 1}{\omega_{\mu\nu} - \omega_{\mathbf{k}}} \hat{a}_{\mathbf{k}} + \frac{e^{i(\omega_{\mu\nu} + \omega_{\mathbf{k}})t} - 1}{\omega_{\mu\nu} + \omega_{\mathbf{k}}} \hat{a}_{\mathbf{k}}^{\dagger} \right] |\xi_{\nu}(0)\rangle \right] , \quad (\text{A12})$$

where

$$\omega_{\mu\nu} = \omega_\mu - \omega_\nu. \quad (\text{A13})$$

We define the *atomic density operator* ρ as the trace of the full density operator $\psi\psi^\dagger$ with respect to the radiation states. For the matrix elements $\rho_{\mu\nu} = \langle \mu | \rho | \nu \rangle$ we obtain by a straightforward calculation

$$\rho_{\mu\nu} = \langle \xi_\nu | \xi_\mu \rangle. \quad (\text{A14})$$

Combining (A14) with (A7) we get the following expression for the time derivative of the density-matrix elements:

$$\begin{aligned} \frac{d\rho_{\mu\nu}}{dt} = & -i\omega_{\mu\nu}\rho_{\mu\nu} \\ & + \sum_{\mathbf{k}} \sum_{\lambda} (g_{\mathbf{k}\mu\lambda} \langle \xi_\nu | \hat{a}_{\mathbf{k}} - \hat{a}_{\mathbf{k}}^\dagger | \xi_\lambda \rangle \\ & - g_{\mathbf{k}\lambda\nu} \langle \xi_\lambda | \hat{a}_{\mathbf{k}} - \hat{a}_{\mathbf{k}}^\dagger | \xi_\mu \rangle). \end{aligned} \quad (\text{A15})$$

The radiation field consists of the coherent laser field plus the spontaneous radiation. We consider the free-field propagator $e^{-i\hat{\Omega}\tau}$ acting on the wave function with τ positive and much larger than the optical period. Since

the spontaneously emitted radiation travels outwards from the origin, the result appears as a pure multimode coherent state if the radiation field is measured at the origin. In other words, the wave function fulfills the relation

$$\sum_{\mathbf{k}} \mathbf{f}_{\mathbf{k}} \hat{a}_{\mathbf{k}} e^{-i\hat{\Omega}\tau} \psi = \sum_{\mathbf{k}} \mathbf{f}_{\mathbf{k}} \alpha_{\mathbf{k}} e^{-i\omega_{\mathbf{k}}\tau} e^{-i\hat{\Omega}\tau} \psi, \quad \tau \gg \tau_{\text{opt}} \quad (\text{A16})$$

where $\alpha_{\mathbf{k}}$ are the coherent-state parameters of the laser field at the time considered. Assuming that (A16) is valid at $t=0$ we find from (A12) that to the first order in the coupling constants we have

$$\begin{aligned} \sum_{\mathbf{k}} \mathbf{f}_{\mathbf{k}} \hat{a}_{\mathbf{k}} | \xi_\mu(t) \rangle \\ = \sum_{\mathbf{k}} \mathbf{f}_{\mathbf{k}} \left[e^{-i\omega_{\mathbf{k}}t} \alpha_{\mathbf{k}} | \xi_\mu(t) \rangle \right. \\ \left. + i \sum_{\nu} g_{\mathbf{k}\mu\nu} \frac{e^{i(\omega_{\nu\mu} - \omega_{\mathbf{k}})t} - 1}{\omega_{\nu\mu} - \omega_{\mathbf{k}}} | \xi_\nu(t) \rangle \right]. \end{aligned} \quad (\text{A17})$$

Using this relation and its Hermitian adjoint, we obtain from (A15) the following set of equations which are correct up to the second order in the coupling constants:

$$\begin{aligned} \frac{d\rho_{\mu\nu}}{dt} = & -i\omega_{\mu\nu}\rho_{\mu\nu} + \sum_{\mathbf{k}} \left\{ \sum_{\lambda} [g_{\mathbf{k}\mu\lambda} (\alpha_{\mathbf{k}} e^{-i\omega_{\mathbf{k}}t} - \alpha_{\mathbf{k}}^* e^{+i\omega_{\mathbf{k}}t}) \rho_{\lambda\nu} - g_{\mathbf{k}\lambda\nu} (\alpha_{\mathbf{k}} e^{-i\omega_{\mathbf{k}}t} - \alpha_{\mathbf{k}}^* e^{+i\omega_{\mathbf{k}}t}) \rho_{\mu\lambda}] \right. \\ & - i \sum_{\lambda\sigma} \left[\left[g_{\mathbf{k}\lambda\nu} g_{\mathbf{k}\mu\sigma} \frac{e^{i(\omega_{\sigma\mu} - \omega_{\mathbf{k}})t} - 1}{\omega_{\sigma\mu} - \omega_{\mathbf{k}}} + g_{\mathbf{k}\mu\sigma} g_{\mathbf{k}\lambda\nu} \frac{e^{i(\omega_{\mathbf{k}} - \omega_{\lambda\nu})t} - 1}{\omega_{\mathbf{k}} - \omega_{\lambda\nu}} \right] \rho_{\sigma\lambda} \right. \\ & \left. \left. - g_{\mathbf{k}\mu\lambda} g_{\mathbf{k}\lambda\sigma} \frac{e^{i(\omega_{\sigma\lambda} - \omega_{\mathbf{k}})t} - 1}{\omega_{\sigma\lambda} - \omega_{\mathbf{k}}} \rho_{\sigma\nu} - g_{\mathbf{k}\lambda\nu} g_{\mathbf{k}\sigma\lambda} \frac{e^{i(\omega_{\mathbf{k}} - \omega_{\sigma\lambda})t} - 1}{\omega_{\mathbf{k}} - \omega_{\sigma\lambda}} \rho_{\mu\sigma} \right] \right\}. \end{aligned} \quad (\text{A18})$$

The first term on the right-hand side of (A18) is of zeroth order in the coupling constants and yields the expected oscillatory behavior of the density-matrix elements between states of different energy. Then comes some first-order terms which involve the coherent-state parameters $\alpha_{\mathbf{k}}$ and represent the stimulated emission and absorption. Equating the expectation value of the laser field to the classical notation of a coherent radiation field

$$\mathbf{E} = \text{Re}(\mathbf{E}_0 e^{i(\mathbf{k}\cdot\mathbf{r} - \omega t)}), \quad (\text{A19})$$

we find the following relation from which all first-order terms in (A18) can be calculated:

$$\sum_{\mathbf{k}} \alpha_{\mathbf{k}} g_{\mathbf{k}\mu\nu} e^{-i\omega_{\mathbf{k}}t} = -\frac{i}{2\hbar} \mathbf{E}_0 \cdot \mathbf{D}_{\mu\nu} e^{-i\omega t}. \quad (\text{A20})$$

The second-order terms of (A18) are responsible for the spontaneous decay. Letting ω_0 denote an unspecified constant, we find that all these second-order terms are of the type

$$\sum_{\mathbf{k}} g_{\mathbf{k}\mu\nu} g_{\mathbf{k}\lambda\sigma} \frac{e^{i(\omega_{\mathbf{k}} - \omega_0)t} - 1}{\omega_{\mathbf{k}} - \omega_0},$$

or the complex conjugate of such a sum. When the quantization volume tends to infinity, the sum tends to an integral which can be written as follows:

$$\begin{aligned} \sum_{\mathbf{k}} g_{\mathbf{k}\mu\nu} g_{\mathbf{k}\lambda\sigma} \frac{e^{i(\omega_{\mathbf{k}} - \omega_0)t} - 1}{\omega_{\mathbf{k}} - \omega_0} \\ = \frac{1}{6\pi^2 \epsilon_0 \hbar c^3} \mathbf{D}_{\mu\nu} \cdot \mathbf{D}_{\lambda\sigma} \int_0^\infty \frac{e^{i(\omega - \omega_0)t} - 1}{\omega - \omega_0} \omega^3 d\omega. \end{aligned} \quad (\text{A21})$$

The imaginary part of this integral can be calculated for large time values (as compared to the optical period) by using the formal relation

$$\frac{\sin[(\omega - \omega_0)t]}{\omega - \omega_0} d\omega \rightarrow \pi \delta(\omega - \omega_0) \quad \text{as } t \rightarrow \infty. \quad (\text{A22})$$

The real part of the integral only gives rise to a (small) shift of the energy levels (part of the Lamb shift), which we assume to be included in the measured transition frequency. Disregarding this shift we get, except in a negligibly small time interval, the following result which yields all second-order terms in (A18):

$$\begin{aligned} \sum_{\mathbf{k}} g_{\mathbf{k}\mu\nu} g_{\mathbf{k}\lambda\sigma} \frac{e^{i(\omega_{\mathbf{k}} - \omega_0)t} - 1}{\omega_{\mathbf{k}} - \omega_0} \\ = \begin{cases} i\pi\omega_0^3 \mathbf{D}_{\mu\nu} \cdot \mathbf{D}_{\lambda\sigma} / (6\pi^2 \hbar \epsilon_0 c^3) & \text{if } \omega_0 > 0 \\ 0 & \text{if } \omega_0 < 0. \end{cases} \end{aligned} \quad (\text{A23})$$

We shall now assume that there are two degenerate levels 1 and 2 with energies $\hbar\omega_1$ and $\hbar\omega_2$, respectively. The states of these levels are labeled $(1m)$ and $(2m)$, respectively, where m is the magnetic quantum number. Furthermore, we assume that level 1, which is lower than level 2, in metastable, i.e., it is not dipole coupled to any lower levels. On the other hand, level 2 may be dipole coupled both to level 1 and to other levels. (We do not allow cascade transitions from level 2 to level 1.) For the sake of simplicity we assume that the levels that are higher than level 2 do not participate and can be left out completely in the calculations.

It is seen from the zeroth-order approximation that the density-matrix element $\rho_{\mu\nu}$ oscillates with the angular velocity $\omega_{\mu\nu}$. In the resonance approximation we retain in (A18) only terms oscillating with almost the same angular velocity, since only such terms can, when integrated, yield significant contributions to $\rho_{\mu\nu}$. The effect of the resonance approximation on the first-order terms in (A18) is that only transitions in resonance with the laser field are induced. We shall restrict our treatment to the case where the laser only induces transitions between the states of the levels 1 and 2 mentioned above. Using the spherical tensor components, which for a general vector \mathbf{A} are given by

$$A^{(1)} = -(A_x + iA_y) / \sqrt{2}, \quad (\text{A24a})$$

$$A^{(0)} = -A_z, \quad (\text{A24b})$$

$$A^{(-1)} = (A_x - iA_y) / \sqrt{2}, \quad (\text{A24c})$$

we can write the scalar product between the dipole moment and the polarization vector

$$\mathbf{E}_0 \cdot \mathbf{D}_{1m,2m'} = \sum_{q=-1}^1 (-1)^q \mathbf{E}_0^{(-q)} D_{1m,2m'}^{(q)}. \quad (\text{A25})$$

If the laser is linearly polarized in the direction of the quantization axis, only the $q=0$ component is nonzero. In the same way, the two circular polarizations are represented by $q=\pm 1$ (with a quantization axis along the beam). The right-hand side of (A25) is nonzero only if the difference between the m quantum numbers of the states is equal to q , and consequently, only such transitions are induced by the laser.

As concerns the second-order terms in (A18), which give rise to the spontaneous decay of the upper level, it is easily seen that the matrix element $\rho_{\mu\nu}$ is "spontaneously coupled" only to matrix elements between states such

that the energy difference is (almost) equal to $\hbar\omega_{\mu\nu}$. To reduce further the number of states involved we express the scalar product of the dipole moments in (A23) in terms of the spherical tensor components defined in (A24a)–(A24c). Remembering that only one of these components can be nonzero for a given set of m values, we obtain the following relation, where the numbers 1–4 denote four arbitrary levels and δ is the Kronecker delta:

$$\begin{aligned} \mathbf{D}_{1m_1,2m_2} \cdot \mathbf{D}_{3m_3,4m_4} \\ = \delta_{m_1-m_2, m_4-m_3} (-1)^q D_{1m_1,2m_2}^{(m_1-m_2)} D_{3m_3,4m_4}^{(m_2-m_1)}. \end{aligned} \quad (\text{A26})$$

This means that the scalar product of two dipole moments can be nonzero only if the difference between the m quantum numbers is the same for both moments. Since no levels higher than level 2 are excited and level 1 is metastable, it follows that the equations we need to calculate the diagonal elements $\rho_{1m,1m}$ and $\rho_{2m,2m}$ can be written as follows:

$$\begin{aligned} \frac{d\rho_{1m,1m}}{dt} = & -e^{-i\omega t} v_m \rho_{1m,2(m-q)} - e^{i\omega t} v_m^* \rho_{2(m-q),1m} \\ & + 2 \sum_{m'} \gamma_{m',m} \rho_{2m',2m'}, \end{aligned} \quad (\text{A27a})$$

$$\begin{aligned} \frac{d\rho_{2m,2m}}{dt} = & e^{-i\omega t} v_{m+q} \rho_{1(m+q),2m} \\ & + e^{i\omega t} v_{m+q}^* \rho_{2m,1(m+q)} - 2\gamma \rho_{2m,2m}, \end{aligned} \quad (\text{A27b})$$

$$\begin{aligned} \frac{d\rho_{1m,2(m-q)}}{dt} = & e^{i\omega t} v_m^* (\rho_{1m,1m} - \rho_{2(m-q),2(m-q)}) \\ & + (i\omega_{21} - \gamma) \rho_{1m,2(m-q)}, \end{aligned} \quad (\text{A27c})$$

where q is given by the laser polarization and

$$v_m = (-1)^{q+1} \frac{i}{2\hbar} \mathbf{E}_0^{(q)} D_{2(m-q),1m}^{(-q)}, \quad (\text{A28})$$

$$\gamma_{m,m'} = \frac{1}{6\pi\hbar\epsilon_0 c^3} \omega_{21}^3 |D_{1m',2m}|^2, \quad (\text{A29})$$

$$\gamma = \frac{1}{6\pi\hbar\epsilon_0 c^3} \sum_{\omega_\mu < \omega_2} \omega_{2\mu}^3 |D_{\mu,2m}|^2. \quad (\text{A30})$$

Here the Rabi frequencies v_m can be taken real and positive without essential restriction since their phases only determine the phase of the nondiagonal density-matrix elements. The parameter $\gamma_{m,m'}$ can be interpreted as the decay rate from the state $2m$ to the particular state $1m'$, whereas γ represents the total decay rate for the $2m$ state to all lower levels. These quantities are easily related to the lifetime of level 2 and the branching ratio for transition from level 2 to level 1 by means of the Wigner-Eckart theorem.

¹I. I. Rabi, Phys. Rev. **51**, 652 (1937).

²R. H. Dicke, Phys. Rev. **93**, 99 (1954).

³E. L. Hahn, Phys. Rev. **80**, 580 (1950).

⁴H. C. Torrey, Phys. Rev. **76**, 1059 (1949).

⁵F. Bloch, Phys. Rev. **70**, 460 (1946).

⁶R. P. Feynman, F. L. Vernon, and R. W. Hellwarth, J. Appl. Phys. **28**, 49 (1957).

⁷G. B. Hocker and C. L. Tang, Phys. Rev. Lett. **21**, 591 (1968).

- ⁸R. G. Brewer and R. L. Shoemaker, *Phys. Rev. Lett.* **27**, 631 (1971).
- ⁹P. M. Farrell, W. R. MacGillivray, and M. C. Standage, *Phys. Lett.* **107A**, 263 (1985).
- ¹⁰J. E. Golub, Y. S. Bai, and T. W. Mossberg, *Phys. Rev. A* **37**, 119 (1988).
- ¹¹H. M. Gibbs, *Phys. Rev. A* **8**, 446 (1973).
- ¹²D. Scarl, L. A. Hackel, M. A. Johnson, and M. C. Rushford, *Phys. Rev. A* **24**, 883 (1981).
- ¹³S. Avrillier, J.-M. Raimond, Ch. J. Bordé, D. Bassi, and G. Scoles, *Opt. Commun.* **39**, 311 (1981).
- ¹⁴J. P. C. Kroon, H. A. J. Senhorst, H. C. W. Beijerinck, B. J. Verhaar, and N. F. Verster, *Phys. Rev. A* **31**, 3724 (1985).
- ¹⁵A. G. Adam, T. E. Gough, N. R. Isenor, and G. Scoles, *Phys. Rev. A* **32**, 1451 (1985).
- ¹⁶A. Wännström, O. Vogel, A. Arnesen, R. Hallin, A. Kastberg, C. Nordling, and S. Linnaeus, *Phys. Rev. A* **38**, 5964 (1988).
- ¹⁷O. Vogel, Ph.D. thesis, University of Uppsala, Sweden, 1987 [Acta Univ. Ups. Nova Acta Regiae Soc. Sci. Ups. Ser. V.C. **106**, 1987].
- ¹⁸S. L. Kaufman, *Opt. Commun.* **17**, 309 (1976).
- ¹⁹W. H. Wing, G. A. Ruff, W. E. Lamb, and J. J. Spezeski, *Phys. Rev. Lett.* **36**, 1488 (1976).
- ²⁰See, e.g., R. Loudon, *The Quantum Theory of Light* (Clarendon, Oxford, 1983).
- ²¹B. W. Shore, *Phys. Rev. A* **17**, 1739 (1978).
- ²²S. Stenholm, *Foundations of Laser Spectroscopy* (Wiley, New York, 1984).
- ²³J. Reader, C. H. Corliss, W. L. Wiese, and G. A. Martin, *Wavelengths and Transitions Probabilities for Atoms and Atomic Ions*, Natl. Bur. Stand. Ref. Data Ser., Natl. Bur. Stand. (U. S.) Circ. No. 68 (U.S. GPO, Washington, D.C., 1980), Vol. X.
- ²⁴T. D. Gaily, M. J. Coggiola, J. R. Peterson, and K. T. Gillen, *Rev. Sci. Instrum.* **51**, 1168 (1980).
- ²⁵N. Bendali, H. T. Duong, J. M. Saint Jalm, and J. L. Vialie, *J. Phys. (Paris)* **44**, 1019 (1983).
- ²⁶U. Nielsen, O. Poulsen, and L. Young, *Opt. Lett.* **10**, 591 (1985).
- ²⁷B. Wellegehausen and H. H. Heitmann, *Appl. Phys. Lett.* **34**, 44 (1979).
- ²⁸Ph. Cahuzac and R. Vetter, *Phys. Rev. A* **14**, 270 (1976).
- ²⁹R. L. Shoemaker and E. W. van Stryland, *J. Chem. Phys.* **64**, 1733 (1976).
- ³⁰A. Wännström, O. Vogel, A. Arnesen, and R. Hallin, *Phys. Scr.* **38**, 564 (1988).
- ³¹H. Hühnermann, K. Dörschel, T. Meier, and H. Wagner, *Nucl. Instrum. Methods B* **26**, 435 (1987).
- ³²S. H. Autler and C. H. Townes, *Phys. Rev.* **100**, 703 (1955).
- ³³J. L. Picqué and J. Pinard, *J. Phys. B* **9**, L77 (1976).
- ³⁴H. R. Gray and C. R. Stroud, *Opt. Commun.* **25**, 359 (1978).
- ³⁵See, e.g., P. T. H. Fisk, H. A. Bachor, and R. J. Sandeman, *Phys. Rev. A* **33**, 2418 (1986).
- ³⁶Y. S. Bai, T. W. Mossberg, N. Lu, and P. R. Berman, *Phys. Rev. Lett.* **57**, 1692 (1986).
- ³⁷L. Allen and J. H. Eberly, *Optical Resonance and Two-Level Atoms* (Wiley, New York, 1975).
- ³⁸M. M. T. Loy, *Phys. Rev. Lett.* **32**, 814 (1974).